Landslides
DOI 10.1007/s10346-020-01461-z
Received: 19 December 2019
Accepted: 10 June 2020

Susumu Nakajima · Keita Abe · Masahiro Shinoda · Susumu Nakamura · Hidetaka Nakamura

Experimental study on impact force due to collision of rockfall and sliding soil mass caused by seismic slope failure

Abstract A series of the experiments was conducted to understand the effect of weight, size, shape, stiffness, material of collision object, and type of movement of collision object on mobilization characteristics of impact force. Results from the element rockfall test, rockfall test using slope model, are introduced in the paper. The relationships between the maximum amplitude of the impact force and the momentum were highly scattered depending on the shape, stiffness, constituent material, and type of the movement of the collision object. On the other hand, the results obtained from the tests indicated that the relationships between force product and momentum of the impact load can be expressed by single linear equation with high coefficient of determination although the test conditions were largely different. The knowledge obtained from the reduced scale tests, which are element rockfall test and rockfall test using slope model, extended to the prototype scale by referring to the results of the dynamic centrifuge model test and pendulum test conducted by authors and others. By reflecting these knowledges, a concept of the energy-based design approach, which makes it possible to rationalize the design of the protection wall for rockfall and sliding soil mass, is also proposed.

Keywords Rockfall · Energy-based design approach · Impact force · Protection wall

Introduction

Background

Recently, the slope failure and rockfall cause the loss of safety, loss of human life, and eventual damage of infrastructure because of heavy rainfall and large earthquake in Japan (Nakamura et al. 2014; Nakajima et al. 2019; Nishimura et al. 2020). It is very difficult, however, to conduct a precise risk evaluation or a retrofitting work with detailed ground survey for all slope close to the infrastructure and houses. Thus, a construction of protection wall is a solution to protect the infrastructures and human life (Volkwein et al. 2011).

These protection walls are required to have sufficient internal and external stability even though there is a lack of enough knowledge on mobilization characteristics of impact load due to collision of rockfall or sliding soil mass induced by slope failure. The material, shape, weight, size and stiffness of the collision object, type of movement of collision object, and stiffness of the protection wall would affect the mobilization characteristics of impact force. The comprehensive knowledge on the effect of change of these affecting factors on the mobilization characteristics of impact force has not been obtained yet as reviewed in the next section.

Previous study

To rationalize the design procedure of the protection wall, it is necessary to understand the mobilization characteristics of the impact force which is affected by many factors as mentioned above. Many experimental and analytical studies have been carried out in order to investigate the above phenomenon. Reduced scale model tests are conducted to obtain basic knowledge on the impact force due to the collision of rockfall, sliding soil mass induced by slope failure and debris flow (e.g., Nakatsutsumi and Tani 1982; Nakano and Ukon 1986; Labiouse and Heidenreich 2009; Buzzi et al. 2012; Glover 2015). Full-scale tests and back analysis of the actual event are also carried out to enhance knowledge obtained from reduced scale model tests. There are several works that aim to develop a procedure to evaluate the maximum impact force based on the full-scale test and centrifuge model test on rockfall phenomena (Chikatamarla et al. 2004; Perret et al. 2004; Francesco et al. 2005; Peila et al. 2007; Wang and Cavers 2008; Yu and Zhao 2018; Yu et al. 2019). Lambert and Kister (2018) proposed an empirical criterion for evaluating the capacity of existing rockfall protection embankment based on a literature survey of real-scale impact experiments. The proposed criterion relates deformation of embankment to the maximum kinetic energy.

The author's research work also reached to the evaluation of the impact force. Using an artificial large-scale slope, The authors conducted a series of model tests to investigate flow behavior and to evaluate the impact force due to soil flow and rockfall(Abe and Nakamura 2017; Nakamura et al. 2018). The results indicated that the empirical equation based on fluid mechanics underestimated the impact force in cases where it was applied to evaluate the impact force due to the flow of solid geomaterial and rockfall.

As reviewed above, there are many studies conducting experiments, analyses on rockfall phenomena, and debris flow although there are no experimental studies that aim to clarify the effect of collision material and types of movement on the mobilization characteristics of impact force. Moreover, there is no experimental study evaluating impact force due to the collision of sliding soil mass caused by earthquake-induced slope failure to the structure in prototype scale.

Study objectives and outline of paper

Based on the background and considering the knowledge obtained by the previous study, series of the experiment that are named as element rockfall test and rockfall test using slope model are conducted to investigate the effect of the shape, material, stiffness, size of the collision object, and stiffness of the facing of the protection wall on the impact force. The objective and outline of the study is schematically illustrated in Fig. 1. This study aims to understand the effect of various factors on mobilization characteristics of impact force by conducting element rockfall test. In the "Element

Published online: 24 July 2020

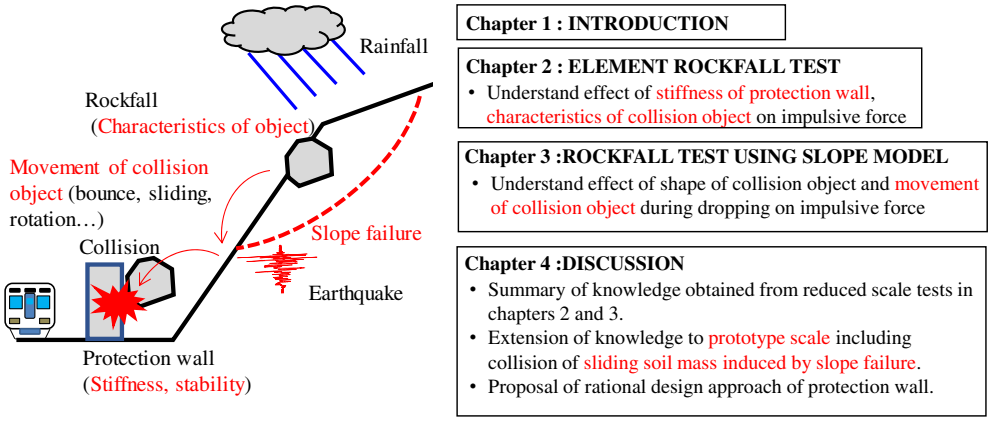

Fig. 1 Outline of study

rockfall test" section, the effect of the characteristics of collision object (weight, size, shape, stiffness, and material) and stiffness of the protection wall on the impact load are investigated through the simplest movement condition (i.e., vertical free fall). In the "Rockfall test using slope model" section, the shape of collision object and type of moving during the falling of the collision material on mobilization characteristics of impact force is investigated based on the results of rock fall test using slope model, in which moving type of collision object consists of several types, although only vertical free fall is the case in element rock fall test discussed in the "Element rock fall test" section. In the "Discussion" section, the knowledge on the impact load obtained from element rock fall test and rock fall test using slope model is summarized. The relevant studies in the prototype scale which are pendulum test simulating rockfall phenomena and dynamic centrifuge model test on the impact of sliding soil mass caused by slope failure are also discussed to extend knowledge obtained from reduced scale tests discussed in the "Element rock fall test" and "Rockfall test using slope model" sections. Applying the knowledge obtained from the study, a rational design methodology of protection wall based on energy approach is proposed.

Element rock fall test

Outline of test

The authors conducted a series of element rockfall tests to investigate the effect of (1) shape and size (diameters of 0.2 m and 0.4 m) of dropping object, (2) deformation and strength characteristics of dropping object, and (3) stiffness of structure subjected to impact load. In the element rockfall test, models of rock and soil mass is dropped onto the reaction unit, which are supported by five H-shaped steel piles with length of 5 m containing three-component load cell. The outline of the test is schematically illustrated in Fig. 2. Test conditions are summarized in Tables 1, 2, 3, and 4. The width, length, and height of reaction unit are 1.4, 2.6, and 1.2 m, respectively. The impact load perpendicular to the collision as well as the vertical direction are also measured with small interference of 1.92% and small eccentric error of 1.0% in dynamic condition by using the three-component load cell. Additionally, a plate made of concrete or wood is used as the facing material of the load cell to investigate the effect of facing stiffness of the protection wall on the impact force.

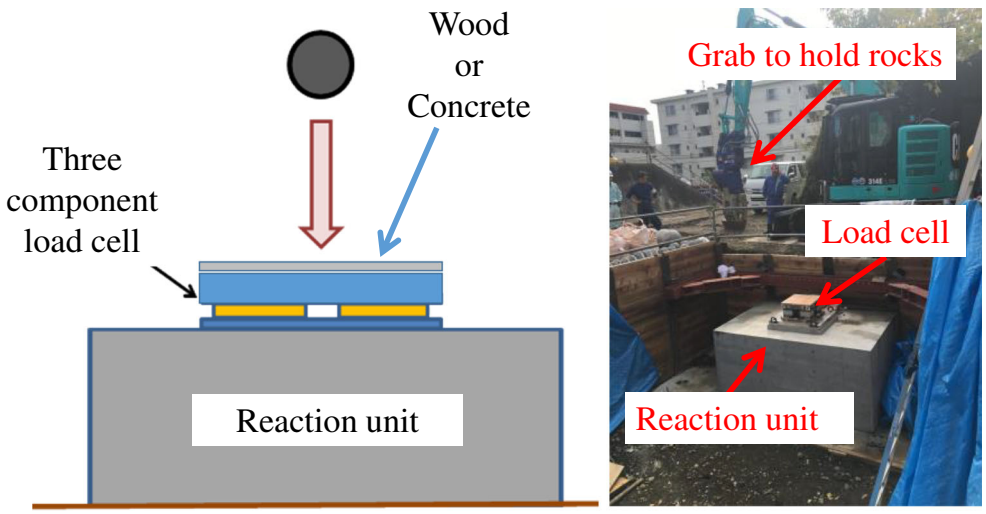

Fig. 2 Elemental free fall test

Table 1 Summary of test condition and result on deformable soil (named as soil test series)

Test number	Facing condition	Weight (kN)	Height (m)	Impact force (kN)	Fdt (kNs)	V (m/s)	Mv (kNs)
Soil(1) 177	Wood	1.57	1.00	88	0.88	4.42	0.71
Soil(1) 178	Wood	1.57	0.99	83	0.87	4.40	0.70
Soil(1) 179	Wood	1.57	3.00	154	1.47	7.68	1.23
Soil(1) 180	Wood	1.57	3.00	147	1.50	7.67	1.23
Soil(1) 181	Wood	1.57	4.00	108	1.65	8.86	1.42
Soil(1) 182	Wood	1.57	4.02	180	1.70	8.88	1.42
Soil(1) 183	Wood	1.57	4.02	163	1.67	8.88	1.42
Soil(2) 160	Wood	0.39	1.01	30	0.22	4.45	0.18
Soil(2) 161	Wood	0.39	3.01	113	0.36	7.69	0.31
Soil(2) 162	Wood	0.39	3.00	113	0.36	7.67	0.31
Soil(2) 163	Wood	0.39	5.01	179	0.45	9.91	0.40
Soil(2) 165	Wood	0.39	5.01	121	0.46	9.91	0.40
Soil(2) 166	Wood	0.78	0.99	52	0.43	4.41	0.35
Soil(2) 167	Wood	0.78	3.00	129	0.71	7.67	0.61
Soil(2) 168	Wood	0.78	2.99	210	0.72	7.66	0.61
Soil(2) 169	Wood	0.78	2.98	150	0.72	7.65	0.61
Soil(2) 170	Wood	0.78	5.01	167	0.91	9.91	0.79
Soil(2) 171	Wood	0.78	4.99	221	0.91	9.89	0.79
Soil(2) 172	Wood	1.18	0.99	119	0.69	4.41	0.53
Soil(2) 173	Wood	1.18	3.00	89	1.09	7.66	0.92
Soil(2) 174	Wood	1.18	3.01	127	1.10	7.68	0.92
Soil(2) 175	Wood	1.18	4.99	275	1.39	9.89	1.19
Soil(2) 176	Wood	1.18	5.00	387	1.39	9.90	1.19
Soil(3) 158	Wood	0.98	3.04	69	0.77	7.72	0.77
Soil(3) 159	Wood	0.98	3.03	85	0.85	7.71	0.77
Soil(1) 136	Concrete	1.57	0.99	48	0.82	4.41	0.71
Soil(1) 137	Concrete	1.57	0.98	40	0.80	4.38	0.70
Soil(1) 138	Concrete	1.57	3.00	168	1.43	7.67	1.23
Soil(1) 139	Concrete	1.57	2.99	130	1.40	7.66	1.23
Soil(1) 141	Concrete	1.57	4.00	117	1.67	8.86	1.42
Soil(1) 142	Concrete	1.57	3.99	152	1.69	8.85	1.42
Soil(2) 126	Concrete	0.39	0.98	51	0.21	4.38	0.18
Soil(2) 127	Concrete	0.39	2.98	168	0.32	7.65	0.31
Soil(2) 128	Concrete	0.39	2.99	110	0.36	7.65	0.31
Soil(2) 130	Concrete	0.39	5.00	110	0.46	7.65	0.31
Soil(2) 131	Concrete	0.39	4.98	79	0.45	9.88	0.40
Soil(2) 143	Concrete	0.78	1.00	56	0.44	4.43	0.35
Soil(2) 144	Concrete	0.78	3.00	100	0.74	7.67	0.61
Soil(2) 145	Concrete	0.78	3.01	159	0.75	7.68	0.61
Soil(2) 146	Concrete	0.78	5.01	118	0.94	9.92	0.79
Soil(2) 147	Concrete	0.78	5.00	235	0.93	9.91	0.79
Soil(2) 118	Concrete	1.18	1.01	151	0.69	4.45	0.53

Table 1 (continued)

Test number	Facing condition	Weight (kN)	Height (m)	Impact force (kN)	Fdt (kNs)	V (m/s)	Mv (kNs)
Soil(2) 120	Concrete	1.18	2.99	198	1.14	7.66	0.92
Soil(2) 125	Concrete	1.18	2.98	164	1.15	7.64	0.92
Soil(2) 123	Concrete	1.18	5.01	230	1.41	9.92	1.19
Soil(2) 124	Concrete	1.18	4.99	278	1.41	9.89	1.19
Soil(3) 114	Concrete	0.98	3.01	74	0.88	7.69	0.77
Soil(3) 135	Concrete	0.98	2.98	76	1.46	7.64	0.76

In the rockfall test, as shown in Figs. 3 and 4, three types of materials are used as the dropping objects that are (1) natural rocks obtained from a construction site, (2) models of rock with different shapes, and (3) deformable soil which can be regarded as the sliding soil.

Natural rock and models of rock with different shapes are shown in Fig. 3. Two types of rock models whose shape are spherical and block are constructed with mortar mixing fiber synthetics. The block shape model is constructed to coincide with the typical shape of natural rock by making the formwork of the selected natural rock. Deformable soil is also used as the dropping object in this study to investigate the effect of deformation and strength characteristics of dropping object on trends of impact load mobilization. Three different methodologies are adopted to drop the deformable soil as schematically illustrated in Fig. 4.

Test result and discussion

Typical time histories of the impact force obtained during the collision of spherical rock model with a length of 20 cm to the concrete and wooden facing are shown in Fig. 5. The maximum

Table 2 Summary of test conditions and results on rock model of sphere shape (named as SP test series)

Test number	Facing condition	Weigh (kN)	Height (m)	Impact force(kN)	Fdt (kNs)	V (m/s)	mv (kNs)
SP 24	Wood	0.09	0.99	44	0.06	4.41	0.04
SP 23	Wood	0.09	2.00	23	0.03	6.27	0.06
SP 22	Wood	0.09	2.99	97	0.11	7.66	0.07
SP 31	Wood	0.09	3.04	112	0.12	7.72	0.07
SP 21	Wood	0.09	4.01	109	0.12	8.87	0.08
SP 184	Wood	0.09	5.01	157	0.14	9.91	0.09
SP 29	Wood	0.70	0.48	127	0.31	3.07	0.22
SP 38	Wood	0.70	0.52	113	0.31	3.19	0.23
SP 28	Wood	0.70	0.99	490	0.53	4.41	0.32
SP 39	Wood	0.70	1.01	215	0.45	4.44	0.32
SP 27	Wood	0.70	2.01	587	0.70	6.28	0.45
SP 25	Wood	0.70	3.01	494	0.79	7.68	0.55
SP 30	Wood	0.70	3.00	1020	0.93	7.67	0.55
SP 32	Wood	0.70	2.99	602	0.81	7.66	0.55
SP 91	Concrete	0.70	0.49	417	0.38	3.10	0.22
SP 92	Concrete	0.70	0.49	417	0.38	3.10	0.22
SP 93	Concrete	0.70	1.01	535	0.48	4.46	0.32
SP 108	Concrete	0.09	1.00	109	0.08	4.43	0.04
SP 94	Concrete	0.70	2.00	758	0.62	6.26	0.45
SP 110	Concrete	0.09	2.00	148	0.11	6.26	0.06
SP 95	Concrete	0.70	2.50	871	0.67	7.00	0.50
SP 111	Concrete	0.09	3.00	198	0.13	7.67	0.07
SP 112	Concrete	0.09	4.01	275	0.14	8.87	0.08
SP 113	Concrete	0.09	5.01	249	0.15	9.91	0.09

Table 3 Summary of test condition and result on rock model of block shape (named as BL test series)

Test number	Facing condition	Weight (kN)	Height (m)	Impact force (kN)	Fdt (kNs)	V (m/s)	mV (kNs)
BL 41	Wood	0.08	1.00	41	0.05	4.43	0.04
BL 45	Wood	0.08	1.00	32	0.05	4.43	0.04
BL 49	Wood	0.08	1.00	36	0.05	4.44	0.04
BL 33	Wood	0.08	3.00	68	0.09	7.67	0.06
BL 42	Wood	0.08	3.03	70	0.09	7.71	0.06
BL 46	Wood	0.08	3.00	89	0.10	7.67	0.06
BL 50	Wood	0.08	3.02	62	0.08	7.69	0.06
BL 43	Wood	0.08	4.00	74	0.10	8.86	0.07
BL 47	Wood	0.08	4.02	80	0.10	8.88	0.07
BL 51	Wood	0.08	3.99	68	0.10	8.85	0.07
BL 53	Wood	0.08	3.99	61	0.09	8.84	0.07
BL 55	Wood	0.08	3.98	80	0.10	8.84	0.07
BL 57	Wood	0.08	4.00	90	0.10	8.85	0.07
BL 59	Wood	0.08	3.99	71	0.09	8.85	0.07
BL 44	Wood	0.08	5.00	92	0.12	9.90	0.08
BL 48	Wood	0.08	5.01	97	0.12	9.92	0.08
BL 52	Wood	0.08	4.99	120	0.13	9.89	0.08
BL 54	Wood	0.08	5.00	88	0.11	9.90	0.08
BL 56	Wood	0.08	5.00	74	0.10	9.90	0.08
BL 58	Wood	0.08	5.00	101	0.12	9.90	0.08
BL 60	Wood	0.08	5.00	120	0.12	9.90	0.08
BL 104	Wood	0.31	1.00	71	0.16	4.44	0.14
BL 110	Wood	0.31	0.99	65	0.18	4.40	0.14
BL 114	Wood	0.31	1.00	81	0.19	4.44	0.14
BL 34	Wood	0.31	2.99	165	0.32	7.66	0.25
BL 106	Wood	0.31	2.99	165	0.28	7.66	0.25
BL 111	Wood	0.31	3.00	188	0.32	7.66	0.25
BL 115	Wood	0.31	3.00	188	0.23	7.68	0.25
BL 108	Wood	0.31	4.01	157	0.24	8.87	0.28
BL 112	Wood	0.31	4.02	208	0.25	8.87	0.28
BL 118	Wood	0.31	4.00	176	0.31	8.86	0.28
BL 122	Wood	0.31	3.97	190	0.27	8.83	0.28
BL 124	Wood	0.31	4.00	178	0.24	8.85	0.28
BL 126	Wood	0.31	3.98	173	0.25	8.84	0.28
BL 128	Wood	0.31	3.97	182	0.29	8.83	0.32
BL 109	Wood	0.31	4.99	231	0.25	9.89	0.32
BL 113	Wood	0.31	4.98	269	0.38	9.89	0.32
BL 121	Wood	0.31	4.96	242	0.31	9.87	0.32
BL 123	Wood	0.31	4.97	308	0.40	9.88	0.32
BL 125	Wood	0.31	4.96	273	0.33	9.87	0.32
BL 127	Wood	0.31	4.98	247	0.34	9.88	0.32
BL 130	Wood	0.31	4.96	273	0.34	9.86	0.32

Table 3 (continued)

Test number	Facing condition	Weight (kN)	Height (m)	Impact force (kN)	Fdt (kNs)	V (m/s)	mV (kNs)
BL 29	Concrete	0.08	1.00	73	0.06	4.44	0.04
BL 96	Concrete	0.08	0.99	70	0.06	4.40	0.04
BL 30	Concrete	0.08	0.98	76	0.06	4.39	0.04
BL 31	Concrete	0.08	0.99	98	0.07	4.40	0.04
BL 32	Concrete	0.08	0.98	79	0.06	4.38	0.04
BL 33	Concrete	0.08	0.99	74	0.06	4.41	0.04
BL 36	Concrete	0.08	0.99	72	0.06	4.40	0.04
BL 37	Concrete	0.08	1.00	104	0.06	4.42	0.04
BL 38	Concrete	0.08	0.98	52	0.07	4.39	0.04
BL 39	Concrete	0.08	0.99	70	0.06	4.40	0.04
BL 40	Concrete	0.08	0.99	106	0.07	4.41	0.04
BL 41	Concrete	0.08	1.00	68	0.06	4.42	0.04
BL 34	Concrete	0.08	1.00	63	0.06	4.42	0.04
BL 35	Concrete	0.08	1.00	62	0.06	4.44	0.04
BL 42	Concrete	0.08	3.00	131	0.23	7.67	0.06
BL 43	Concrete	0.08	3.01	107	0.10	7.68	0.06
BL 97	Concrete	0.08	2.99	156	0.11	7.66	0.06
BL 44	Concrete	0.08	4.00	128	0.09	8.86	0.07
BL 98	Concrete	0.08	3.99	154	0.08	8.84	0.07
BL 99	Concrete	0.08	5.01	108	0.12	9.91	0.08
BL 100	Concrete	0.08	4.99	145	0.12	9.89	0.08
BL 45	Concrete	0.31	1.00	205	0.10	4.43	0.14
BL 46	Concrete	0.32	1.01	116	0.20	4.45	0.14
BL 47	Concrete	0.32	1.01	209	0.21	4.46	0.14
BL 48	Concrete	0.32	3.00	383	0.31	7.68	0.25
BL 49	Concrete	0.32	3.02	145	0.28	7.70	0.25
BL 50	Concrete	0.32	3.02	237	0.27	7.70	0.25
BL 51	Concrete	0.32	4.01	164	0.30	8.87	0.29
BL 52	Concrete	0.32	4.02	223	0.20	8.88	0.29
BL 58	Concrete	0.32	4.00	334	0.30	8.85	0.28
BL 59	Concrete	0.32	4.00	351	0.29	8.86	0.29
BL 60	Concrete	0.32	4.00	133	0.26	8.85	0.29
BL 61	Concrete	0.32	4.01	245	0.23	8.87	0.29
BL 62	Concrete	0.32	3.99	308	0.34	8.85	0.29
BL 55	Concrete	0.32	5.01	165	0.25	9.91	0.32
BL 66	Concrete	0.32	4.99	320	0.34	9.89	0.32
BL 56	Concrete	0.32	5.03	373	0.32	9.93	0.32
BL 57	Concrete	0.32	5.01	252	0.23	9.91	0.32
BL 63	Concrete	0.32	5.00	330	0.29	9.91	0.32
BL 64	Concrete	0.32	4.99	288	0.39	9.89	0.32
BL 67	Concrete	0.32	5.00	229	0.19	9.91	0.32

Table 4 Summary of test condition and results on Real Rock (named as RR test series)

Test number	Facing condition	Weight (kN)	Height (m)	Impact force (kN)	Fdt (kNs)	V (m/s)	mV (kNs)
RR 61	Wood	0.12	1.00	43	0.07	4.42	0.05
RR 65	Wood	0.12	1.00	39	0.07	4.44	0.05
RR 69	Wood	0.12	1.00	43	0.16	4.41	0.05
RR 35	Wood	0.12	3.00	112	0.13	7.68	0.09
RR 62	Wood	0.12	3.00	99	0.13	7.66	0.09
RR 66	Wood	0.12	3.00	56	0.09	7.66	0.09
RR 70	Wood	0.12	3.00	53	0.07	7.64	0.09
RR 63	Wood	0.12	4.00	73	0.13	8.83	0.11
RR 67	Wood	0.12	4.00	82	0.14	8.85	0.11
RR 71	Wood	0.12	4.00	72	0.12	8.84	0.11
RR 74	Wood	0.12	4.00	71	0.09	8.86	0.11
RR 76	Wood	0.12	4.00	71	0.12	8.86	0.11
RR 79	Wood	0.12	4.00	63	0.10	8.85	0.11
RR 81	Wood	0.12	4.00	112	0.15	8.86	0.11
RR 64	Wood	0.12	5.00	101	0.15	9.88	0.12
RR 68	Wood	0.12	5.00	101	0.16	9.91	0.12
RR 72	Wood	0.12	5.00	94	0.15	9.88	0.12
RR 75	Wood	0.12	5.00	113	0.14	9.90	0.12
RR 78	Wood	0.12	5.00	92	0.14	9.90	0.12
RR 80	Wood	0.12	5.00	85	0.12	9.92	0.12
RR 82	Wood	0.12	5.00	149	0.18	9.89	0.12
RR 84	Wood	0.12	5.00	103	0.13	9.90	0.12
RR 131	Wood	0.33	1.00	92	0.17	4.44	0.15
RR 137	Wood	0.33	1.00	63	0.16	4.42	0.15
RR 142	Wood	0.33	1.00	98	0.17	4.40	0.15
RR 36	Wood	0.33	3.00	246	0.44	7.66	0.26
RR 132	Wood	0.33	3.00	147	0.26	7.66	0.26
RR 138	Wood	0.33	3.00	224	0.29	7.68	0.26
RR 143	Wood	0.33	3.00	208	0.30	7.66	0.26
RR 133	Wood	0.33	4.00	243	0.33	8.86	0.30
RR 139	Wood	0.33	4.00	315	0.36	8.85	0.30
RR 144	Wood	0.33	4.00	173	0.29	8.87	0.30
RR 146	Wood	0.33	4.00	264	0.34	8.86	0.30
RR 149	Wood	0.33	4.00	160	0.24	8.86	0.30
RR 151	Wood	0.33	4.00	229	0.34	8.84	0.30
RR 154	Wood	0.33	4.00	204	0.29	8.86	0.30
RR 136	Wood	0.33	5.00	358	0.39	9.89	0.34
RR 141	Wood	0.33	5.00	252	0.35	9.89	0.34
RR 145	Wood	0.33	5.00	505	0.43	9.90	0.34
RR 147	Wood	0.33	5.00	423	0.42	9.91	0.34
RR 150	Wood	0.33	5.00	344	0.39	9.88	0.34

Table 4 (continued)

Test number	Facing condition	Weight (kN)	Height (m)	Impact force (kN)	Fdt (kNs)	V (m/s)	mV (kNs)
RR 153	Wood	0.33	5.00	277	0.36	9.89	0.34
RR 155	Wood	0.33	5.00	254	0.35	9.89	0.34
RR 9	Concrete	0.12	0.99	145	0.09	4.40	0.05
RR 101	Concrete	0.13	0.99	69	0.06	4.41	0.06
RR 10	Concrete	0.12	0.98	118	0.08	4.38	0.05
RR 17	Concrete	0.12	0.99	142	0.06	4.40	0.05
RR 18	Concrete	0.12	1.00	105	0.08	4.42	0.05
RR 19	Concrete	0.12	0.99	94	0.09	4.40	0.05
RR 22	Concrete	0.12	1.00	110	0.08	4.43	0.05
RR 23	Concrete	0.12	1.00	98	0.03	4.42	0.05
RR 24	Concrete	0.12	0.98	165	0.10	4.38	0.05
RR 26	Concrete	0.12	0.99	136	0.09	4.41	0.05
RR 27	Concrete	0.12	0.98	136	0.09	4.40	0.05
RR 11	Concrete	0.12	0.97	110	0.08	4.36	0.05
RR 12	Concrete	0.12	0.99	120	0.09	4.41	0.05
RR 25	Concrete	0.12	1.01	123	0.10	4.44	0.05
RR 14	Concrete	0.12	2.99	200	0.14	7.65	0.09
RR 103	Concrete	0.13	2.99	103	0.08	7.66	0.10
RR 28	Concrete	0.12	3.98	410	0.18	8.84	0.11
RR 104	Concrete	0.13	4.01	120	0.09	8.86	0.11
RR 106	Concrete	0.13	4.99	184	0.13	9.89	0.13
RR 107	Concrete	0.13	4.99	171	0.11	9.90	0.13
RR 70	Concrete	0.33	1.00	155	0.12	4.43	0.15
RR 68	Concrete	0.33	1.00	149	0.13	4.44	0.15
RR 69	Concrete	0.33	1.01	149	0.13	4.46	0.15
RR 71	Concrete	0.33	3.00	257	0.21	7.67	0.26
RR 72	Concrete	0.33	3.00	246	0.25	7.67	0.26
RR 73	Concrete	0.33	3.01	353	0.27	7.68	0.26
RR 74	Concrete	0.43	3.98	276	0.33	8.83	0.39
RR 75	Concrete	0.43	4.00	322	0.29	8.86	0.39
RR 77	Concrete	0.43	3.99	285	0.21	8.84	0.39
RR 78	Concrete	0.43	4.00	416	0.32	8.85	0.39
RR 80	Concrete	0.27	4.00	441	0.33	8.86	0.24
RR 81	Concrete	0.27	4.00	192	0.19	8.86	0.24
RR 82	Concrete	0.27	3.99	260	0.31	8.84	0.24
RR 83	Concrete	0.27	4.99	341	0.24	9.89	0.27
RR 84	Concrete	0.27	4.98	416	0.32	9.88	0.27
RR 87	Concrete	0.28	5.02	125	0.25	9.92	0.29
RR 88	Concrete	0.28	5.00	255	0.23	9.90	0.29
RR 85	Concrete	0.27	4.97	334	0.27	9.88	0.27
RR 89	Concrete	0.28	4.98	292	0.25	9.89	0.29
RR 90	Concrete	0.28	5.00	215	0.21	9.90	0.29

Table 5 Summary of test condition of rock fall test using large-scale slope model

Test number	Weight (kN)	Slope condition	Impact force (kN)	Fdt (kNs)	V (m/s)	mV (kNs)
L-SP 5	0.09		111.69	0.12	7.36	0.07
L-SP 8	0.09		108.02	0.12	7.77	0.07
L-SP 13	0.09		121.77	0.12	6.70	0.06
L-SP 16	0.09		90.59	0.10	7.50	0.07
L-SP 18	0.09		91.11	0.13	7.44	0.07
L-SP 21	0.09		101.84	0.10	7.66	0.07
L-SP 22	0.09		99.93	0.10	7.56	0.07
L-SP 23	0.09		125.52	0.13	9.40	0.09
L-SP 49	0.09		119.05	0.11	6.32	0.06
L-SP 50	0.09		74.63	0.08	5.12	0.05
L-SP 51	0.09		111.77	0.12	9.08	0.08
L-SP 55	0.09		225.59	0.12	8.21	0.08
L-SP 56	0.09		142.06	0.12	7.65	0.07
L-SP 57	0.09		130.30	0.13	7.72	0.07
L-SP 75	0.09	A	148.31	0.08	4.90	0.05
L-SP 76	0.09	A	135.96	0.11	7.22	0.07
L-SP 77	0.09	A	76.99	0.10	5.30	0.05
L-SP 84	0.09	B	42.13	0.05	2.96	0.03
L-SP 92	0.09	A	143.53	0.10	8.45	0.08
L-SP 93	0.09	A	72.13	0.07	5.63	0.05
L-SP 94	0.09	A	47.50	0.07	3.11	0.03
L-SP 96	0.09	A	117.43	0.07	3.14	0.03
L-SP 97	0.09	A	101.84	0.12	5.52	0.05
L-SP 99	0.09	C	146.47	0.10	6.89	0.06
L-SP 100	0.09	C	189.86	0.11	6.89	0.06
L-SP 101	0.09	C	105.59	0.10	5.87	0.05
L-SP 102	0.09	C	139.71	0.11	6.57	0.06
L-SP 103	0.09	C	195.89	0.10	6.48	0.06
L-SP 33	0.71		649.72	0.74	6.90	0.50
L-SP 34	0.71		551.56	0.75	6.47	0.47
L-SP 35	0.71		1416.36	0.85	8.62	0.62
L-SP 36	0.71		412.44	0.59	6.04	0.44
L-SP 63	0.71		323.32	0.52	4.56	0.33
L-SP 64	0.71		363.54	0.51	5.11	0.37
L-SP 65	0.71		590.16	0.69	6.90	0.50
L-SP 98	0.71	A	355.60	0.46	3.56	0.26
L-PL 42	0.11		57.21	0.07	5.41	0.06
L-PL 43	0.11		27.28	0.02	5.59	0.06
L-PL 46	0.11		37.94	0.06	7.66	0.08
L-PL 47	0.11		–	–	7.10	0.08
L-PL 85	0.11	B	–	–	1.88	0.02
L-PL 107	0.11	C	9.93	0.02	3.58	0.04

Table 5 (continued)

Test number	Weight (kN)	Slope condition	Impact force (kN)	Fdt (kNs)	V (m/s)	mV (kNs)
L-PL 38	0.27		–	–	4.25	0.12
L-PL 39	0.27		92.36	0.08	5.23	0.14
L-PL 54	0.27		106.91	0.15	7.55	0.21
L-PL 67	0.27		228.54	0.06	7.79	0.21
L-PL 68	0.27	B	91.11	0.05	3.88	0.11
L-PL 86	0.27	C	92.65	0.08	3.22	0.09
L-PL 7	0.11		35.39	0.06	5.84	0.06
L-PL 11	0.11		39.71	0.07	5.93	0.06
L-PL 12	0.11		25.15	0.04	4.98	0.05
L-PL 15	0.11		45.96	0.07	6.55	0.07
L-PL 27	0.11		34.71	0.06	6.06	0.07
L-PL 28	0.11		45.88	0.04	6.09	0.07
L-BL 9	0.08		33.46	0.07	7.32	0.06
L-BL 10	0.08		27.94	0.06	5.15	0.04
L-BL 14	0.08		49.27	0.07	6.92	0.06
L-BL 17	0.08		105.89	0.07	5.16	0.04
L-BL 19	0.08		41.10	0.07	5.10	0.04
L-BL 20	0.08		56.40	0.06	6.20	0.05
L-BL 25	0.08		105.66	0.10	6.87	0.06
L-BL 26	0.08		52.94	0.07	8.03	0.07
L-BL 29	0.08		48.68	0.11	6.13	0.05
L-BL 30	0.08		76.91	0.07	6.40	0.05
L-BL 31	0.08		45.44	0.06	7.33	0.06
L-BL 41	0.08		103.02	0.08	5.41	0.05
L-BL 45	0.08		32.21	0.06	4.09	0.03
L-BL 58	0.08		51.18	0.06	5.20	0.04
L-BL 59	0.08		53.31	0.04	3.51	0.03
L-BL 60	0.08		42.87	0.05	5.00	0.04
L-BL 61	0.08		34.04	0.04	4.61	0.04
L-BL 62	0.08		26.03	0.04	3.67	0.03
L-BL 69	0.08	D	42.94	0.05	4.79	0.04
L-BL 71	0.08	A	65.44	0.06	5.87	0.05
L-BL 72	0.08	A	35.37	0.05	7.06	0.06
L-BL 73	0.08	A	36.84	0.04	2.84	0.02
L-BL 79	0.08	B	29.27	0.04	2.68	0.02
L-BL 81	0.08	B	20.44	0.02	4.75	0.04
L-BL 82	0.08	B	36.40	0.06	6.30	0.05
L-BL 83	0.08	B	25.00	0.02	2.29	0.02
L-BL 88	0.08	A	38.82	0.02	3.57	0.03
L-BL 90	0.08	A	17.35	0.02	2.62	0.02
L-BL 91	0.08	A	53.09	0.05	4.38	0.04
L-BL 95	0.08	A	26.91	0.04	3.39	0.03

Table 5 (continued)

Test number	Weight (kN)	Slope condition	Impact force (kN)	Fdt (kNs)	V (m/s)	mV (kNs)
L-BL 104	0.08	C	38.90	0.06	5.52	0.05
L-BL 105	0.08	C	92.94	0.06	4.64	0.04
L-BL 106	0.08	C	15.59	0.04	2.57	0.02
L-BL 37	0.31		113.39	0.18	5.96	0.19
L-BL 40	0.31		294.86	0.27	6.31	0.20
L-BL 52	0.31		108.83	0.16	5.05	0.16
L-BL 53	0.31		157.87	0.26	6.01	0.19
L-BL 66	0.31		115.30	0.18	7.29	0.23
L-BL 70	0.31	D	96.84	0.11	4.29	0.14
L-BL 74	0.31	A	99.63	0.13	3.70	0.12
L-BL 87	0.31	B	45.74	0.11	5.75	0.18

impact force and duration of the impact load are different depending on the stiffness of the wall facing although the same rock model is dropped from the same height.

Relationships between the maximum impact force and momentum obtained from the tests on concrete and wooden facings are summarized in Figs. 6 and 7. Vertical component is highlighted in the following discussion, because the object is dropped vertically from just above the load cell in the series of the test. The value of momentum is evaluated by multiplying the mass of the dropping object "m" by the vertical velocity "v" of the dropping object immediately before the collision. The value of velocity immediately before the collisions is evaluated by Eq. (1).

$$v = \sqrt{2gh}. \tag{1}$$

where h (m) is the falling height and g (m/s^2) is the gravitational acceleration.

It is confirmed that the calculated velocities by Eq. (1) are consistent with ones evaluated from an image analysis process by the PTV (particle tracking velocimetry) method. The outline and recent application of the PTV method adopted in this study are summarized in the relevant study (Watanabe et al. 2005). Equations of linear regression of the maximum impact force based on the least square method are also shown in Figs. 6 and 7. The equations are largely different from each other depending on the shapes of the dropping objects as well as the facing conditions of the load cell. As indicated from the inclinations of the equations, the values of the maximum impact force exhibited from the collisions of the dropping objects to the concrete facing are larger than the ones from the collisions to the wooden facing even if the values of the momentum are equal to each other. This is possibly due to the effect of the energy absorption at the wooden facing. In the case of wooden wall facing, larger elastic deformation is expected as compared with the concrete facing because of lower stiffness. In addition, small plastic deformation of the wooden facing and its progress is also observed although it is not observed in the case of concrete facing. Larger elastic deformation, the occurrence of plastic deformation and associated energy absorption effect of

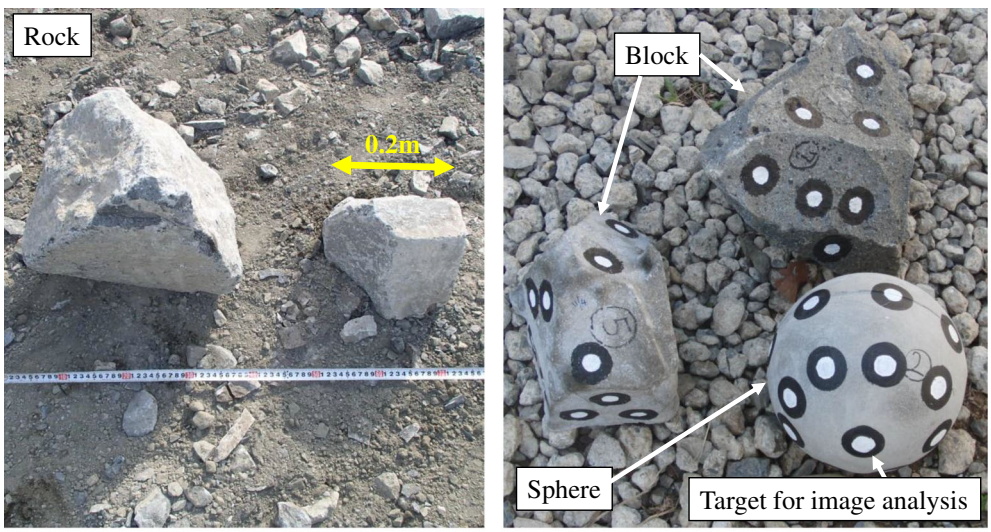

Fig. 3 Natural rock and rock models used in free fall test

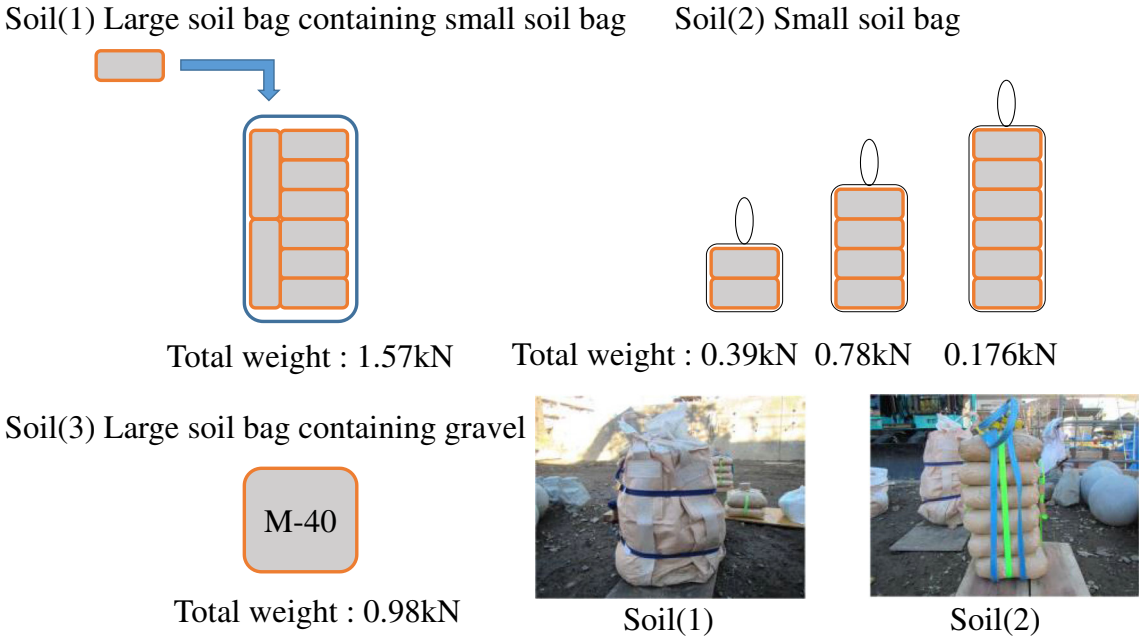

Fig. 4 Test conditions of deformable soil

the wooden facing is thought to be the reason of the observation that the maximum impact force are smaller in the case of the wooden facing as compared to the concrete facing.

The value of the maximum impact force exhibited in the tests on deformable soil is generally smaller than the ones of real rock and rock models. This tendency can be also understood by considering that the soil absorbed the energy by its deformation due to the collisions to the wooden and concrete facing, both of which have much higher strength and stiffness than the deformable soil. In the case of the deformable soil, the effect of the facing rigidity on the relationships between the maximum impact force and momentum is not significant, which also results from the energy absorption due to the deformation of the soil. These results indicate that the energy-based approach is essential to discuss the collision of the rockfall and slope failure–induced sliding soil mass to the structure.

Based on the discussion above, relationships between the value of force product and momentum are shown in Fig. 8. The value of force product is integral of force over time, which can be evaluated as the sum of F_i multiplied by δt, where F_i is the impact force at a certain time and δt is the time increment and the values of force product generated by the first collision are plotted in Fig. 8. The effect of the collisions affected by many factors (e.g., shapes and material consisting of dropping objects, and facing rigidity and strength) can be expressed by single linear equation $F\delta t = 1.18$ mV, where $F\delta t$ is the force product calculated as the integral of force over time, m is the mass of collision object, and V is the velocity of the collision object immediately before the impact to the reaction unit. It should be emphasized that the tests

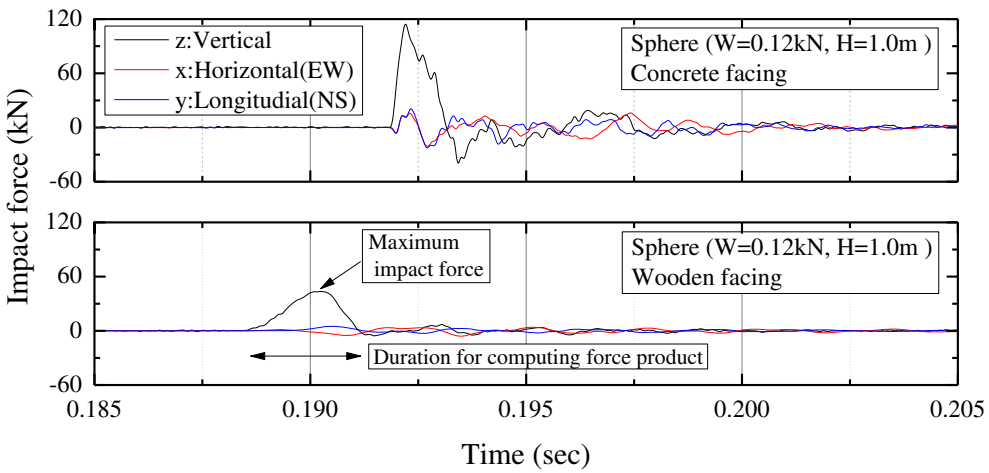

Fig. 5 Example of time histories of impact load

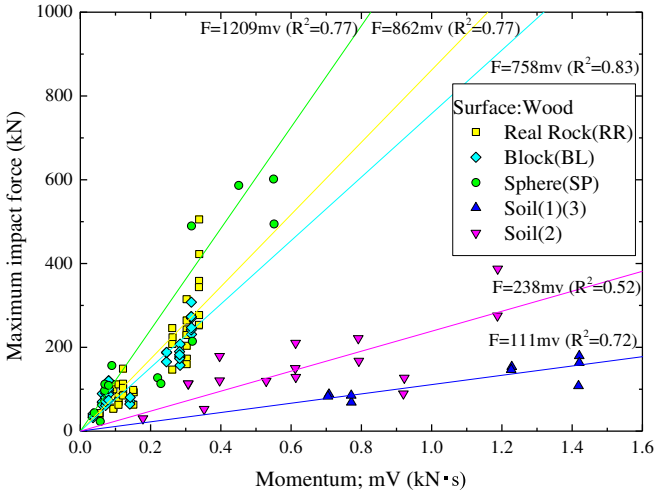

Fig. 6 Relationships between the maximum impact force and momentum in surface condition of wood

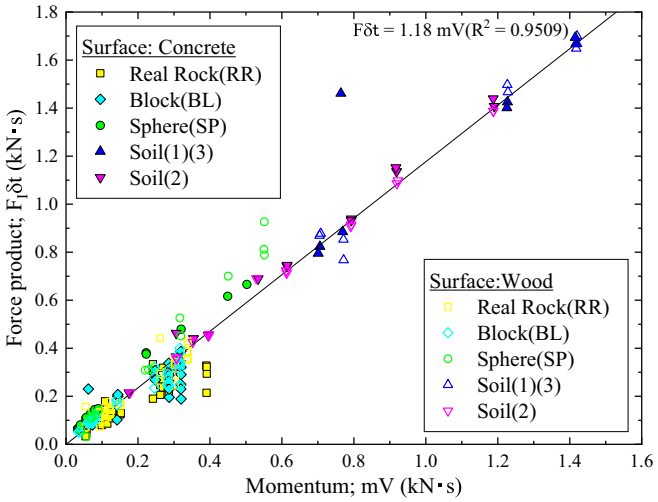

Fig. 8 Relationships between force product and momentum in surface condition of wood

are conducted under a wide variety of conditions in terms of shape, size, and material of the collision object and stiffness of reaction unit. Comparison of Fig. 8 with Figs. 5 and 6 clearly shows that an energy-based approach is more suitable to discuss the effect of collision of rock and soil mass. However, the above knowledge is obtained from the simple free fall experiment, although more complicated behavior composed by sliding, rotation, and reaction at the boundary, as well as free fall is going to be expected in the actual rockfall and sliding of the soils mass caused by slope failure. Thus, the result of the rockfall test using the slope model is discussed in the following chapter.

Rockfall test using slope model

Outline of test

A photo of a slope model with a total length of 10.7 m and a width of 5 m is shown in Fig. 9. A model slope is constructed using the precast concrete board with sufficient strength so as not to deform due to the collisions of the rock model during the test. The slope model consists of three segments. The bottom segment is flat and has a length of 7.5 m. The length and inclination of the bottom part of the slope are 5.7 m and 29 degrees, respectively, and these of the top part is 5.0 m and 43 degrees. Photo of reaction unit is also shown in Fig. 9 and three-component load cell that is the same one used in the element rockfall test is installed in the reaction unit. The plywood board is pasted on the surface of the load cell to avoid damages to the load cell due to the collisions of rock model.

Test conditions are summarized in Table 5. In the series of the tests, spherical, block, and platy shapes of rock models denoted as SP, BL, and PL respectively. Representative lengths of the dropping object are 20 and 40 cm as shown in Fig. 10. The rock models are dropped from the top of the slope model with a height of 1.0 m. Surface condition of the bottom part of the slope is changed in some tests so as to make the movement of the rock model more complicated as shown in Fig. 11, while the surface of the slope is smooth and flat in most of the tests.

Behaviors of the rock models are captured using a high-resolution and speed CCD camera with a sampling frequency of 150 Hz. The velocity of the rock model immediately before the collision to the load cell is evaluated by tracing multiple target points depicted on the surface of rock models.

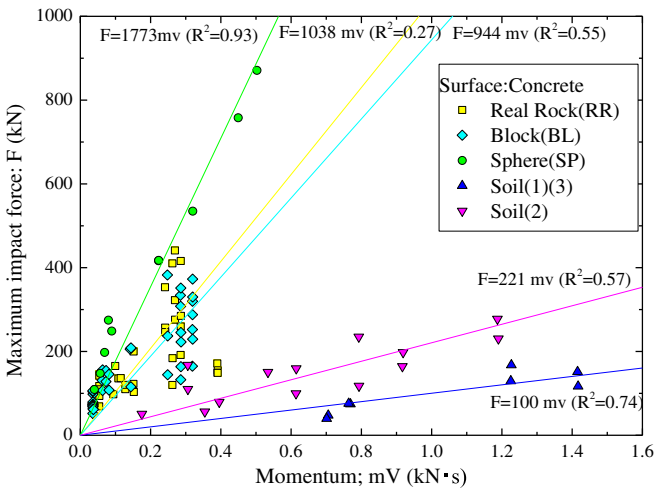

Fig. 7 Relationships between maximum impact force and momentum in surface condition of concrete

Test result and discussion

Typical time histories of impact force due to collision of spherical rock model with their length of 20 cm and 40 cm are shown in Fig. 12. The values of the maximum impact force of horizontal direction (z-direction) increase with the increase of the size of the rock model, and the values of the maximum impact force of the x- and y-direction also increase due to the collision of the rock model. Comparison of the ratio of the maximum impact force in the x- and y-direction to the one in the z-direction in the element rock fall test and rockfall test using the slope model is shown in Fig. 13. It should be emphasized that the measurement of the force from different direction with very small interference and less effect of eccentricity using three-component load cell make it possible to

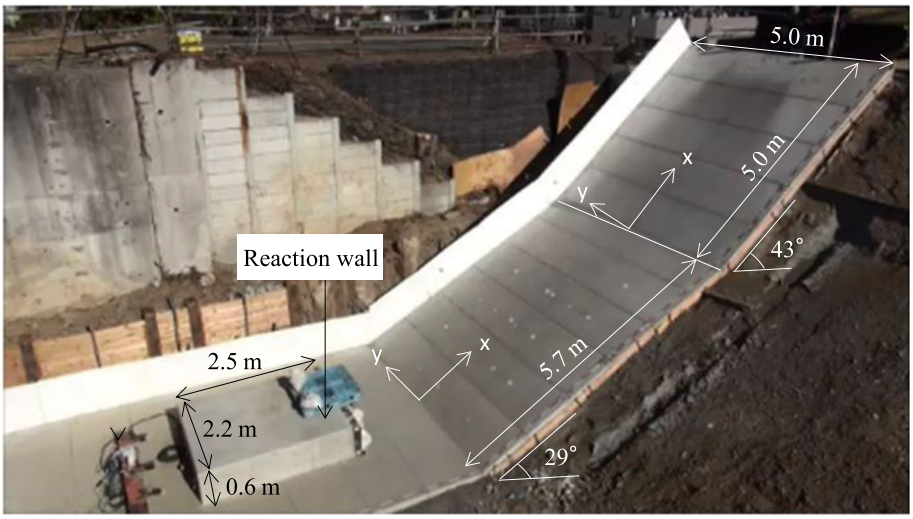

Fig. 9 Large-scale slope model

conduct this kind of the comparison as described in the outline of element rockfall test and rock fall test using large-scale slope model. The weighted average and maximum values of ratio of the maximum impact force of the *x*- and *y*-direction to the horizontal direction (*z*-direction) in element rockfall test are 0.088 and 0.467, while those in the rock fall test using slope model are 0.313 and 0.770. This difference can be understood by considering that the collision object has the velocity component other than the *z*-direction (i.e., *x*- and *y*-direction) in the rockfall test using slope model at impacting the reaction unit because the movement of the collision object in the test consists of sliding, rotation, reaction, and their combination as observed in Abe and Nakamura (2017), Buzzi et al. (2012), and Glover (2015), while the simple free-fall to the reaction unit is the case for the element rockfall test.

The relationship between the maximum impact force and momentum for horizontal direction is summarized in Fig. 14, and the equations of linear regression of the maximum impact force based on the least square method for each dropping object are also shown in the figure. The relationship between the maximum impact force and momentum are affected by the shape of the rock. The maximum impact force induced by the collision of the block and platy rock models is smaller than the one induced by sphere type rock model even if the value of momentum coincides with each other. In the case of the block and plate type model, the edge of the cubic and plate type is chipped due to the collision while no deformation is observed in the case of the spherical model. Energy absorption due to the deformation of the edge of the rock model with the shape of the cubic and plate type model is a possible reason for the above behavior.

The relationship between force product and momentum is shown in Fig. 15. The unique relationship between force product and momentum that are expressed as $F\delta t = 1.34$ mV with R^2 value of 0.9154 can be achieved from all test data obtained from the rockfall test using the slope model although there are limited extents of scattering as compared with element free fall test that are shown in Fig. 8. However, it should be noted that the equation obtained from the rockfall test using slope model corresponds to the equation of $F\delta t = 1.18$ mV that is obtained from the element rockfall test as indicated in Fig. 8.

It is found from the results of the element rockfall test and the rockfall test using slope model that the maximum amplitude of the impact force is significantly affected by many factors, which are shape and size of dropping object, slope condition, rigidity of dropping object itself and reaction unit, and moving

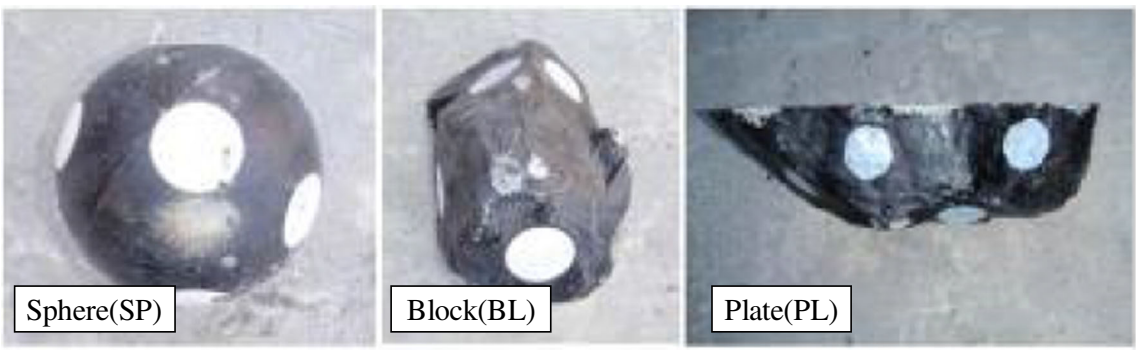

Fig. 10 Shape of rock models

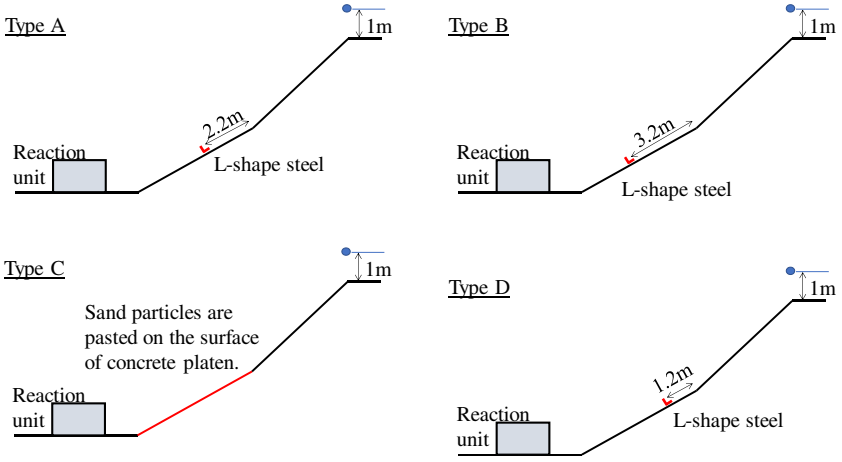

Fig. 11 Arrangement of slope condition

characteristics of dropping object for instances. On the other hand, the relationship between force product and momentum is able to be expressed as a simple linear equation regardless of various test conditions.

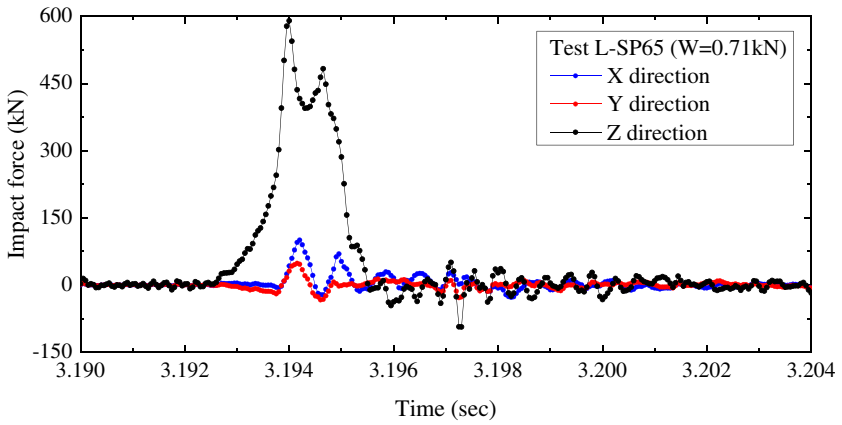

(a) Test L-SP65 (Weight of sphere is 0.71kN)

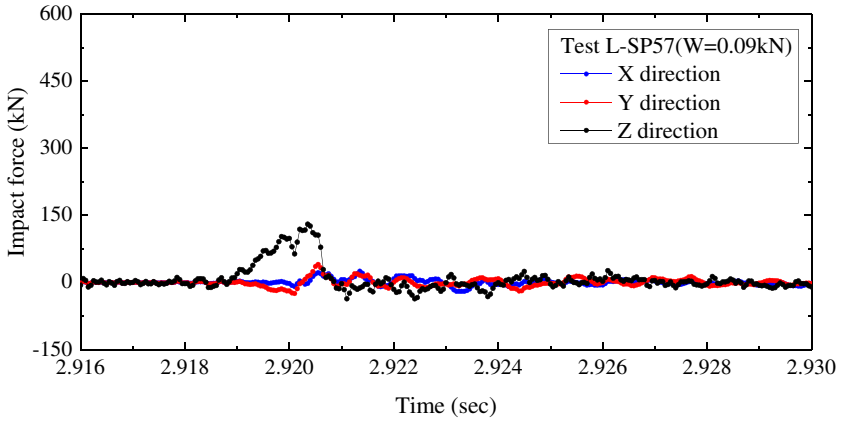

(b) Test L-SP57 (Weight of sphere is 0.09kN)

Fig. 12 Typical time histories of impact force due to the collision of rock model of spherical shape

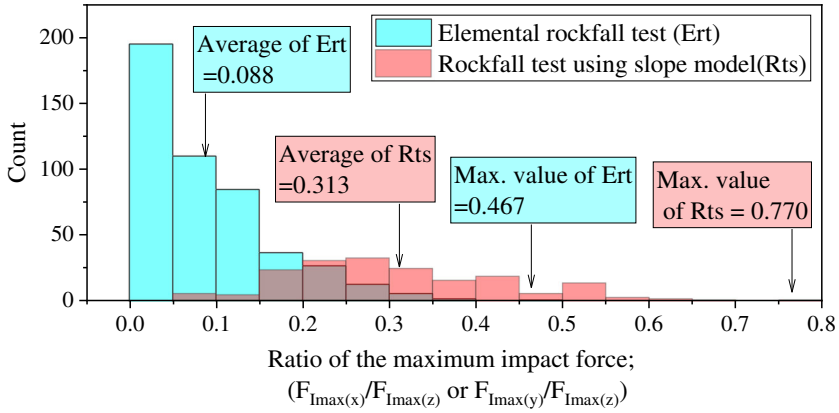

Fig. 13 Comparison of the ratio of the maximum impact force in the *x*- and *y*-direction to the *z*-direction

Discussion

Relevant study conducted in prototype scale

The knowledge obtained from the tests cannot be extended to the problem of the collision of the sliding soil mass induced by the slope failure because the phenomenon close to the rockfall are the main target of the element rockfall tests and the rockfall tests using the slope model. Moreover, the amplitude of the impact force is relatively small as compared to the prototype scale because the abovementioned tests are conducted in a reduced scale. Therefore, the results of the test conducted in the prototype scale are investigated to extend above knowledge to the prototype scale and the problem of the collision of the sliding soil mass to the structure. The analyzed one is the dynamic centrifuge model test of the slope (Nakajima et al. 2019) in which the impact force is due to the collision of the sliding soil mass to the structure. As for the rock fall phenomena with the measurement of the impact force in the prototype scale, a pendulum test (Nishida et al. 2006) is also investigated. After the introduction of the tests in the prototype scale, results obtained from the series of the reduced scale test are compared in this chapter.

Dynamic centrifuge model test

Cross-section of the test is shown in Fig. 16. The height of the slope model is 1000 mm and horizontal shaking is applied under a centrifugal acceleration of 50 g. Therefore, the stress state of the model during shaking corresponds to that of a slope of height 50 m. Table 6 shows the physical and strength parameters of the soil layers used in the experiments. A seismic load, which consists of 10 cycles of sinusoidal excitation at the frequency of 1 Hz, is applied by shaking the soil container horizontally after the centrifugal acceleration of 50 g is applied, while the maximum acceleration of shaking is gradually increased at the increment of about 100 gal in prototype scale.

The failure processes of the slope model in cases 1 and 2 are shown in Fig. 17. In case 1, the surface layer and part of the weak layer showed a sliding failure mode along the failure plane generated in the weak layer in step 5 whose maximum acceleration is 400 gal. Compared with case 1, the failure processes in case 2 commenced at relatively higher acceleration levels in step 6 (α_{max} of 500 gal) and a portion of the surface layer remained on the failure plane, although the lower portion of the surface layer dropped during the failure process in step 7.

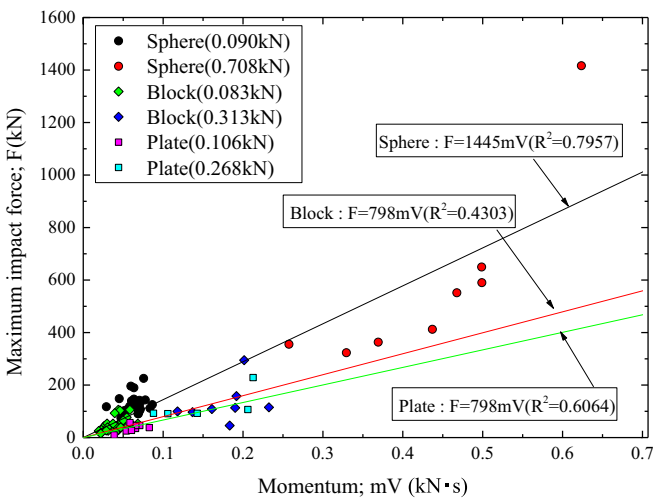

Fig. 14 Relationships between the maximum impact force and momentum

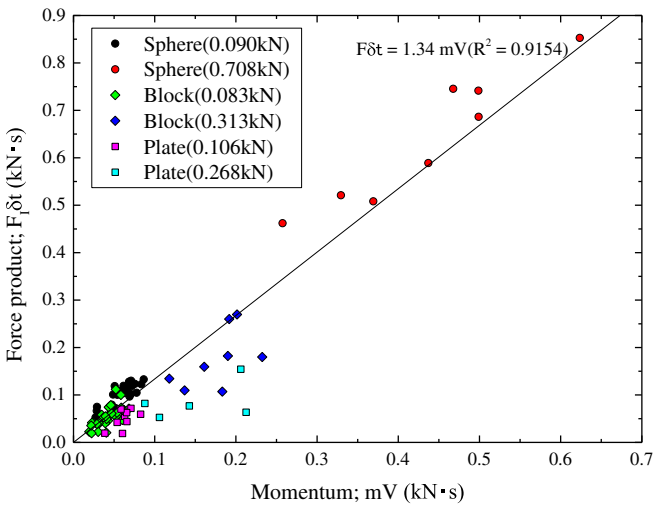

Fig. 15 Relationships between force product and momentum

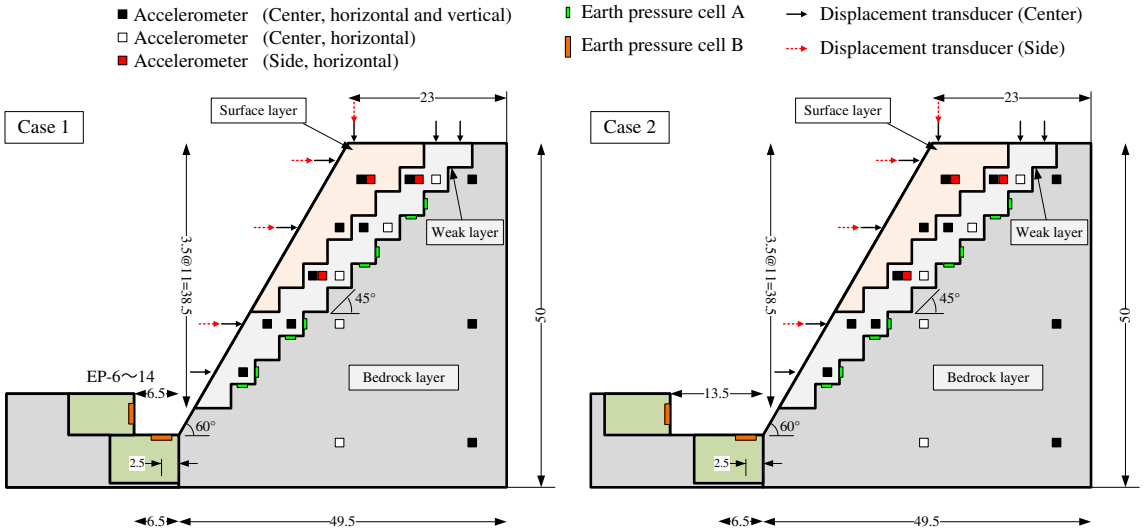

Fig. 16 Prototype cross-sections of slope model in centrifuge model test (unit is in m)

Time histories of the impact force, displacement, and velocity of the sliding soil mass in cases 1 and 2 are summarized in Figs. 18 and 19. The details of the test are written in Nakajima et al. (2019). In the later part of this chapter, a relationship between force product and momentum obtained from the dynamic centrifuge model test is compared with the ones obtained from aforementioned reduced scale model tests.

Pendulum test

In addition to the centrifuge model tests conducted by the authors, a series of pendulum tests conducted by Nishida et al. (2006) is also analyzed in the following discussions as a test result making for the load amplitude obtained by the author's work. Nishida et al. measured impact force by hitting the weight to rockfall protection wall as schematically illustrated

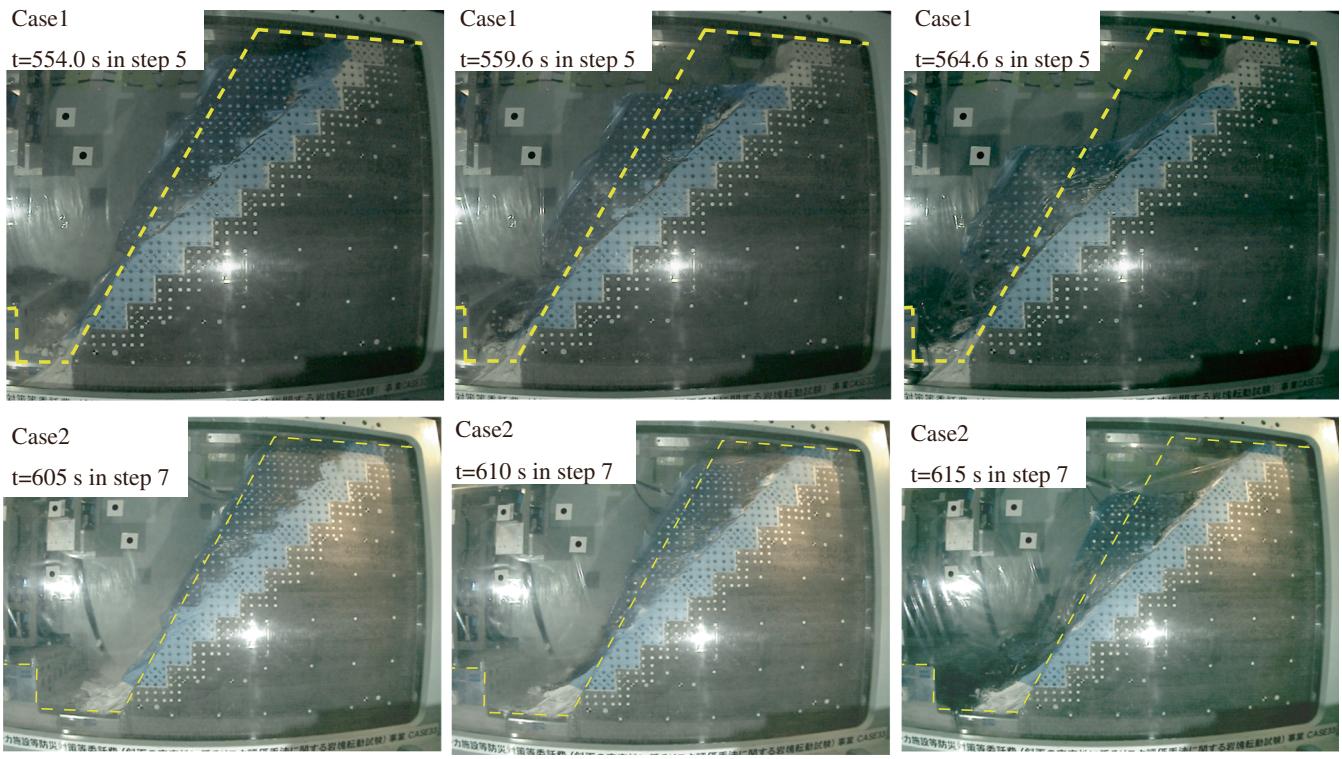

Fig. 17 Failure process of the slope model

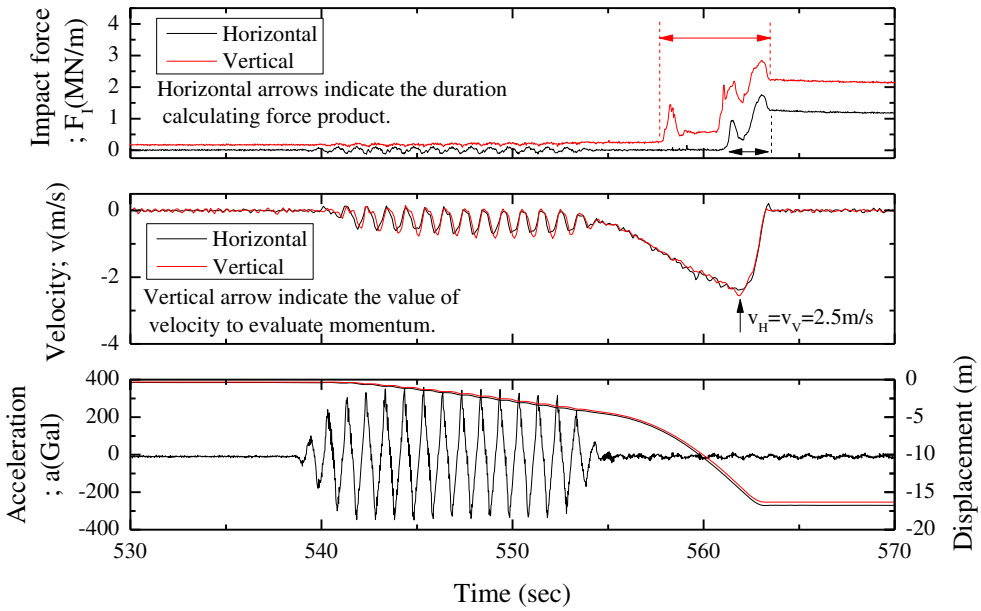

Fig. 18 Time histories of acceleration, relative displacement, and velocity of sliding soil mass and impact force in case 1

in Fig. 20. The protection wall with a height of 2.0 m consists of geosynthetic-reinforced soil and wall facing. The reinforced soil wall is constructed by well-compacted onsite sand with installing the geogrid reinforcement with vertical spacing of 50 cm, which is fixed to the expanded metal facing. A polyester nonwoven geosynthetics with a thickness of 10 mm is pasted on the surface of expand metal. The spherical ball with its weight of 9 kN is made by concrete and it collides against the protection wall with pendulum movement after the weight is released from the height of 11.1 m in case 1 and 20.0 m in case 2 as schematically illustrated in Fig. 20. Three components of accelerometers are installed in the spherical weight and it measured response acceleration due to the collisions of spherical weight to the protection wall.

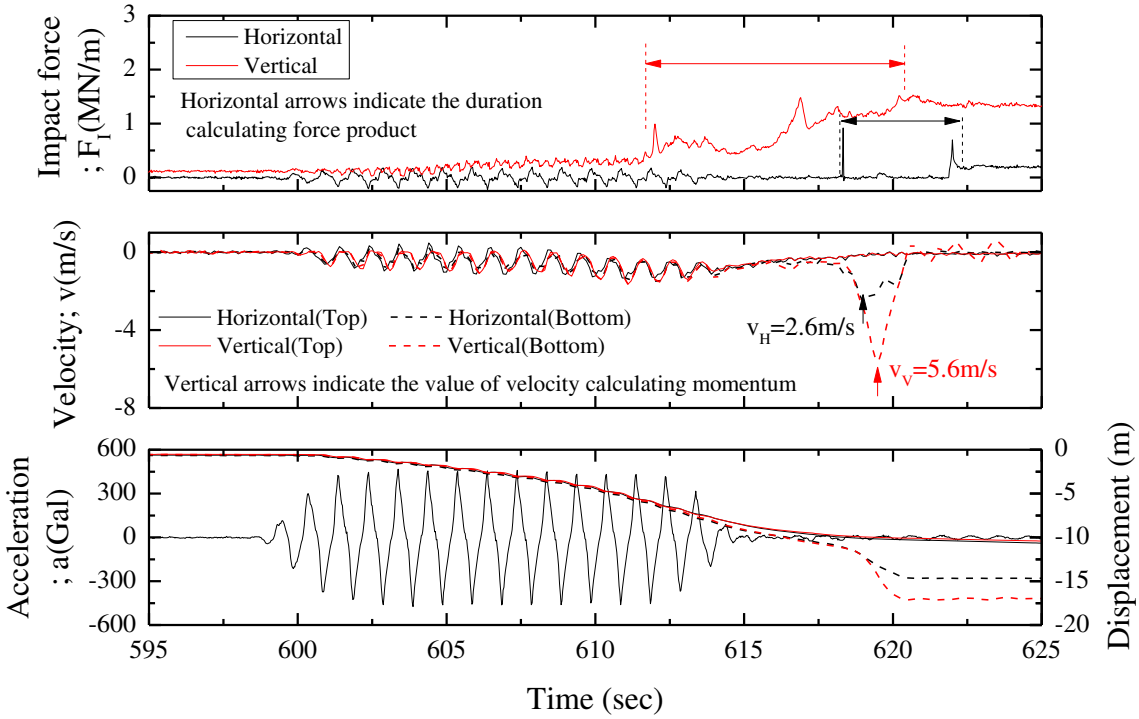

Fig. 19 Time histories of acceleration, relative displacement, and velocity of sliding soil mass and impact force in case 2

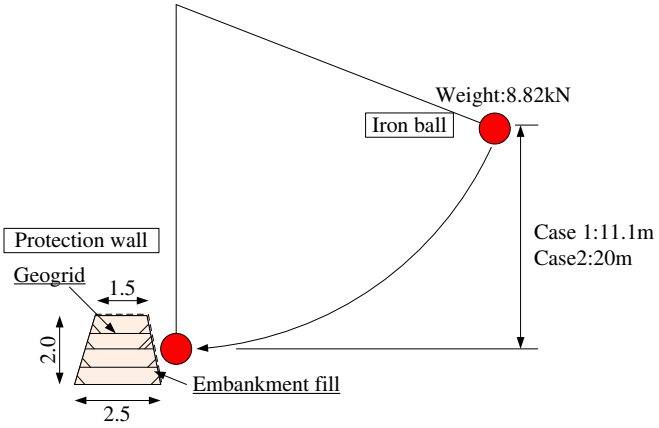

	Case 1	Case 2
Diameter of sphere	0.9 m	
Weight of sphere	8.82 kN	
Initial height	11.1 m	20.0 m
velocity at impact	14.75 m/s	19.80 m/s
Momentum of load	13.27 kNs	17.82 kNs

Fig. 20 Outline of pendulum test conducted by Nishida et.al. (2006)

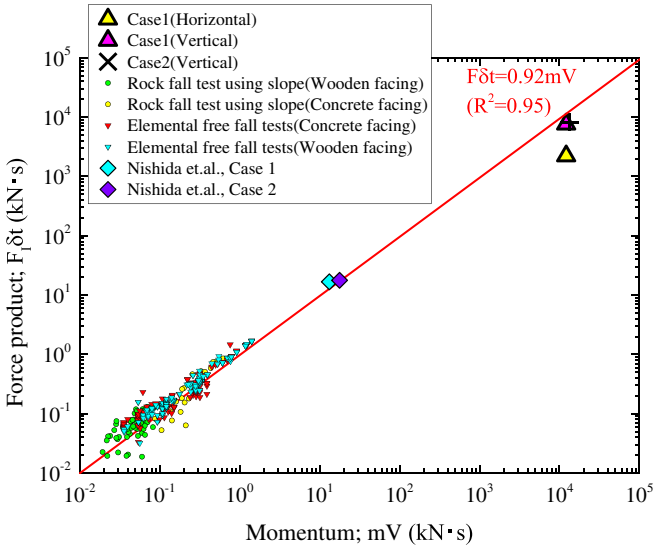

Fig. 22 Summary of relationships between force product and momentum

Time histories of impact force, which are evaluated by multiplying response acceleration to the weight of the sphere, are shown in Fig. 21 and the value of impulse can be obtained in the same manner with the experiments conducted by the authors. The value of momentum can be also evaluated by multiplying the velocity of the weight immediately before the collision to the protection wall to the mass of the spherical weight.

Summary of relationship between force product and momentum

Summary of the relationships between force product and momentum of load of all tests including the pendulum test conducted by Nishida et al. is summarized in Fig. 22. The relationships between force product and momentum of load seem to be expressed by the single linear equation of $F\delta t = 0.92$ mV with high coefficient of determination with its value of 0.95 even though the plotted data are obtained from the tests at a wide variety of conditions.

For the rational design of protection wall against rockfall or sliding soil mass caused by slope failure, deformation of the wall and limited extents of structural damages can be allowed since the maximum amplitude of the load is expected to be very large but the duration of the action is limited. Recently, some sophisticated numerical analyses have made it possible to evaluate a time history of impact force due to the collision of rockfall and sliding soil mass (e.g., Nakajima et al. 2019). By reflecting these knowledges, a direct solution can be possible to evaluate the response of the wall by inputting calculated time history of the impact load as an action but it is too consumptive of time and cost. However, it can be possible to rationalize the design of the protection wall for rockfall and sliding soil mass by reflecting knowledge obtained from the presented study.

Outline of energy-based design of protection wall

In the proposed method, a response of the protection wall located near the toe of the slope can be evaluated by the following steps as schematically illustrated in Fig. 23.

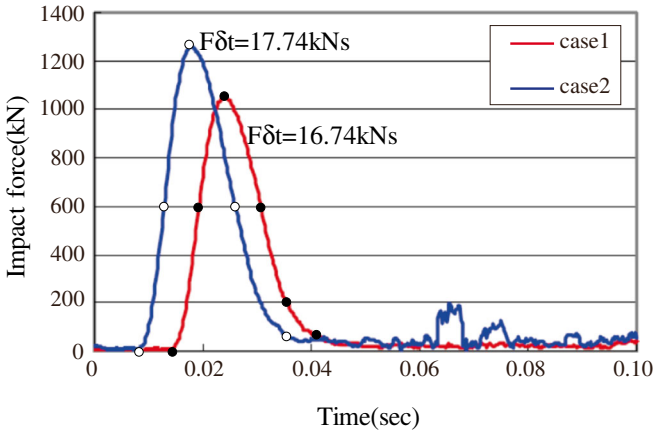

Fig. 21 Typical time histories of impact force obtained from Nishida's study

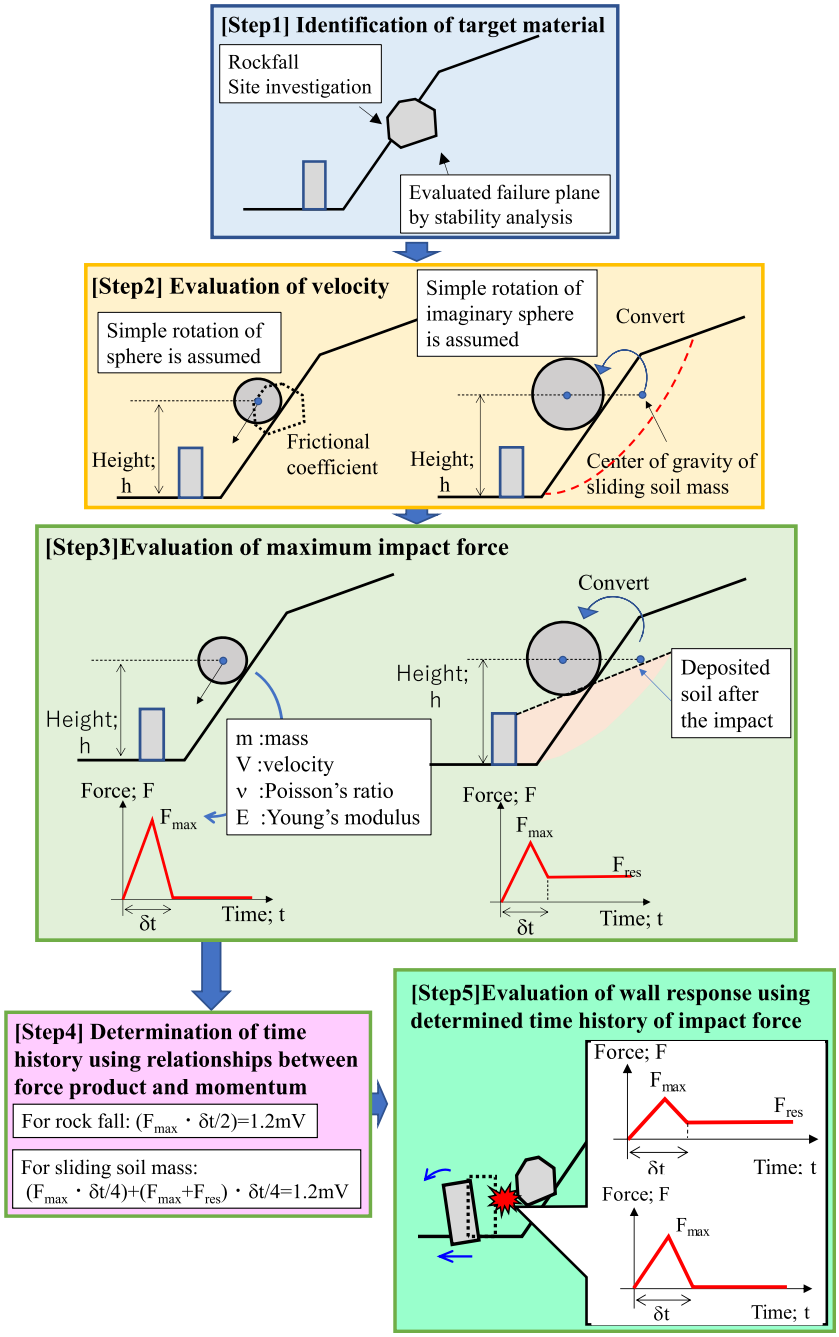

Fig. 23 Outline of proposed method for assessing response of protection wall subjected to impact load

In step 1, a target object is identified. Site investigation is going to find a rock suspected to fall and collide to the protection wall, and stability analysis identifies the possible sliding soil mass. Once the target is identified, the mass of the target can be also evaluated.

In step 2, the value of the velocity at the impact on the protection wall is evaluated. For simplicity, the simple rotation of sphere having the same mass with the original target on the slope is considered in the flow shown in Fig. 23. As observed in the relevant studies by authors and others (Abe et al. 2017; Buzz et al. 2012; Glover 2015, and Zhong et al. 2019), the rock showed multiple forms of movement like sliding, rotating, reaction, and combination of them. These movements are going to affect the vector of the collision object immediately before the impact as well as its amplitude. Therefore, the type of movement of the collision object affects the action acting on the protection wall. In the proposed framework, however, the velocity of the target object is evaluated by assuming the simple rotation of the sphere on the slope. It should be noted that simple rotation of sphere will result in the conservative design because the evaluated velocity will be larger than the case that the movement of the rock and sliding soil mass is precisely simulated.

In Japanese relevant guideline (Japan Road Association 2017) for example, the velocity of the falling object immediately before the impact to the structure is evaluated by Eq. (2), which is based on the free fall assumption.

$$v = \sqrt{2g\left(1-\frac{\mu}{\tan\theta}\right)H}. \quad (2)$$

where v is the velocity of the falling object, g is the gravitational acceleration, μ is the equivalent frictional coefficient whose values are ranging in 0.05 to 0.35 depending on the characteristics of falling object and slope, H is the height of the location where falling object exist, and θ is the angle of the slope.

On the other hand, an analytical approach simulating the movement of the rock (e.g., Perret et al. 2004; Glover 2015) also makes it possible to rationalize the design of the protection wall by giving the reasonable value of velocity.

In step 3, the value of the maximum impact force F_{max} is evaluated using a theoretical equation. Hertz's equation (Hertz 1882) is one of the solutions to calculate the maximum impact force by using Poisson's ratio and Young's modulus of the target object in addition to the mass and velocity evaluated in steps 1 and 2. The value of residual force F_{res} should be also evaluated in case the collision of the sliding soil mass due to the slope failure is considered. The value of F_{res} can be evaluated by considering the volume of deposited soil after the impact. Angle of repose and the location of the failure plane will give the geometry which is essential for the evaluation of the value of F_{res}. Once the geometry after the impact is determined, the value of F_{res} can be evaluated as the active earth pressure using a theoretical equation like Coulomb's equation.

In Fig. 23, the design frame work of the rigid protection wall (e.g., retaining wall consisting of reinforced concrete, Mavrouli and Corominas 2010) is proposed even though the stiffness of the protective measure affects the mobilization characteristics of the impact force as observed in this study. On the other hand, it is effective to apply the other type of the protective measure with high energy absorption ability in case the deformation of the protective measure is accepted (Kwan et al. 2014; Yu et al. 2019). Application of the energy-based design approach is effective in considering the different characteristics of the protective measure.

In step 4, the time history due to the collision of the target object to the protection wall is evaluated. The duration of the impact δt can be easily evaluated by using the relationships between force product and momentum obtained in this study as the equations are indicated in Fig. 23. By reflecting the shape of the time history of the impact obtained by the study, the simple triangle shape is assumed for the collision of the rockfall and square shape determined by the combination of the maximum value F_{max} and residual value F_{res} for the collision of sliding soil mass.

In step 5, the response of the wall is evaluated using the time history of the impact force due to the collision of the target object evaluated in step 4. Recently developed procedures to evaluate seismic-induced residual displacement of the retaining wall (e.g., Nakajima et al. 2009; Railway Technical Research Institute 2012) can be adopted for evaluating the wall response. In the proposed method, it should be emphasized that the design methodology of the protection wall is developed by the combination of rational evaluation of the action on energy-based approach and accepting some extents of displacement or damage of the protection wall considering the collision of rock to the protection wall as the precondition. However, there is the case that the rock bounce over the protection wall, where the impact force is not going to act on the wall but there is another concern that the structure behind the protection wall is affected by the bounced rock. Combination of the proposed method with the reliability analysis evaluating the susceptibility that the bounced rock affects the structure behind the wall makes it possible to consider this type of the phenomena.

Applicability of the proposed method is going to be examined by comparing with the actual behavior and model test in further study.

Conclusions

1 Based on the results from element rockfall test, relationships between force product and momentum could be expressed by linear regression equation of 1.18 for concrete facing and 1.15 for wooden facing with high coefficient of determination value regardless of shape and size of rock model and facing rigidity of load cell although the relationships between the maximum impact force and momentum were significantly affected by these factors.

2 In the rockfall test using slope model, impact forces of vertical and longitudinal component were also recorded as well as horizontal force component because the movement of the rock consisted of rotation, sliding, restitution, and horizontal and vertical displacement although simple free fall movement was the case in the element rockfall test. The average and maximum values of ratio of the maximum impact force of the x- and y-direction to the horizontal direction (z-direction) in element rockfall test are 0.088 and 0.467, while those in the rock fall test using slope model are 0.313 and 0.770.

3 In the rockfall test using slope model, relationships between force product and momentum can be expressed by linear regression with equation of $F\delta t = 1.34$ mV whose R^2 values are 0.9154 although the relationships between the maximum impact force and momentum are highly scattered. The obtained equation from the relationships between the force product and momentum in the rockfall test using slope model corresponded well with the one obtained from the element rockfall test although the scale of the model test was highly different from each other.

4 Results obtained from the elementary rockfall test, rockfall test using slope model, dynamic centrifuge, and pendulum test conducted by Nishida et al. are summarized as the relationships between force product and momentum in this study. It was found from the analysis that all the data could be expressed by linear regression with R^2 of 0.95 although there were limited extents of variations.

5 By reflecting these knowledges, a concept of the energy-based design approach, which makes it possible to rationalize the design of the protection wall for rockfall and sliding soil mass, is also proposed.>

References

Abe K, Nakamura S (2017) Suggestion of evaluation methods of impact loads of rocks and soils based on a series of model experiments, Proc of the 19th International conference on soil mechanics and foundation engineering

Buzzi O, Giacomini A, Spadari M (2012) Laboratory investigation on high values of restitution coefficients. Rock Mech Rock Eng 45(1):35–43
Chikatamarla R, Laue J, Sarah MS (2004) Rockfall impact on protection galleries, second international conference of structural engineering mechanics and computations. Balkema, Rotterdam
Francesco C, di Claudio P, Mauro V (2005) Experimental and numerical study of rock-fall impacts on granular soils. Rivista Italiana di Geotechnica 39(1):95–109
Glover JMH (2015) Rock-shape and its role in rockfall dynamics (Doctoral dissertation, Durham University)
Hertz HZ (1882) On contact between elastic solids, Gsammelte Werke, Vol. 1, Leipzig, Germany
Japan Road Association (2017) Manual of countermeasures for rock fall
Kwan JSH, Chan SL, Cheuk JCY, Koo RCH (2014) A case study on an open hillside landslide impacting on a flexible rockfall barrier at Jordan Valley, Hong Kong. Landslides 11(6):1037–1050
Labiouse V, Heidenreich B (2009) Half-scale experimental study of rockfall impacts on sandy slopes. Nat Hazards Earth Syst Sci 9(6):1981
Lambert S, Kister B (2018) Efficiency assessment of existing rockfall protection embankments based on an impact strength criterion. Eng Geol 243:1–9
Mavrouli O, Corominas J (2010) Vulnerability of simple reinforced concrete buildings to damage by rockfalls. Landslides 7(2):169–180
Nakajima S, Koseki J, Watanabe K, Tateyama M (2009) A simplified procedure to evaluate earthquake-induced residual displacements of conventional type retaining walls. Soils Found 49(2):287–303
Nakajima S, Abe K, Shinoda M, Nakamura S, Nakamura H, Chigira K (2019) Dynamic centrifuge model tests and material point method analysis of the impact force of a sliding soil mass caused by earthquake-induced slope failure. Soils Found 59(6):1813–1819
Nakamura S, Abe K, Wanatabe K, Nakajima S (2018) Analysis of flow and impact behavior based on existing cascading experiment of collapsed soil and reproduction analysis by MPM. J Jpn Soc Civil Eng Ser C (Geosphere Engineering) 74(3):259–274 (in Japanese)
Nakamura S, Wakai A, Umemura J, Sugimoto H, Takeshi T (2014) Earthquake-induced landslides: distribution, motion and mechanisms. Soils Found 54(4):544–559
Nakano M, Ukon N (1986) Experiment on the impact force of collapsed sandy soil mass. J Jpn Soc Erosion Control Eng 39(1):17–23
Nakatsutsumi J, Tani K (1982) Experimental study of impact due to free fall sand. Proceedings of the Japan Society of Civil Engineers 1982:119–127
Nishida Y, Inoue S, Yoshida M, Sawada K, Yashima A (2006) Actual impact test on full scale type model of rock fall protection MSE wall and concrete wall. 41th Ann Cong Jpn Geotech Soc:2237–2238
Nishimura S, Takeshita Y, Nishiyama S, Suzuki S, Shibata T, Shuku T, Komatsu M, Kim B (2020) Disaster report of 2018 July heavy rain for geo-structures and slopes in Okayama, Soils and Foundations (in press)
Peila D, Oggeri C, Castiglia C (2007) Ground reinforced embankments for rockfall protection: design and evaluation of full scale tests. Landslide 4:255–265
Perret S, Dolf F, Kienholz H (2004) Rockfalls into forests: analysis and simulation of rockfall trajectories—considerations with respect to mountainous forests in Switzerland. Landslides 1(2):123–130
Railway Technical Research Institute (2012) Design standard for railway structure - retaining structure-. Maruzen, Tokyo
Volkwein A, Schellenberg K, Labiouse V, Agliardi F, Berger F, Bourrier F, Dorren LKA, Gerber W, Jaboyedoff M (2011) Rockfall characterization and structural protection – a review, natural hazards and earth system science. Science 11:2617–2651
Wang B, Cavers DS (2008) A simplified approach for rockfall ground penetration and impact stress calculations. Landslides 5(3):305
Watanabe K, Koseki J, Tateyama M (2005) Application of high-speed digital CCD cameras to observe static and dynamic deformation characteristics of sand. Geotech Test J ASTM 28(5):423–435
Yu BYW, Zhao H (2018) Experimental study on the maximum impact force by rock fall. Landslide 15:233–242
Yu ZX, Zhao L, Liu YP, Zhao SC, Xu H, Chan SL (2019) Studies on flexible rockfall barriers for failure modes, mechanisms and design strategies: a case study of Western China. Landslides 16(2):347–362
Zhong MJ, Zhi JC, Qing HN, Tian JW, Hao S, Ting HW (2019) Laboratory study on the infuluencing factors and their control for the coefficient of restitution during rockfall impact. Landslides 16(10):1939–1963

S. Nakajima (✉) · **K. Abe**
Railway Technical Research Institute,
2-8-35, Hikarimachi, Kokubunji-shi, Tokyo 185-8530, Japan
Email: nakajima.susumu.99@rtri.or.jp

K. Abe
e-mail: abe.keita.06@rtri.or.jp

M. Shinoda
National Defense Academy,
1-10-20, Hashirimizu, Yokosuka-shi, Kanagawa 239-8686, Japan
e-mail: shinoda@nda.ac.jp

S. Nakamura
Nihon University,
1 Nakagawara, Tokusada, Tamuramachi, Koriyama-shi, Fukushima 963-8642, Japan
e-mail: s-nak@civil.ce.nihon-u.ac.jp

H. Nakamura
Japan Nuclear Authority,
1-9-9, Roppongi, Minato-ku, Tokyo 106-8450, Japan
e-mail: hidetaka_nakamura@nsr.go.jp